Planetary and Space Science 113-114 (2015) 205–218

Contents lists available at ScienceDirect

Planetary and Space Science

journal homepage: www.elsevier.com/locate/pss

Distribution of sulphuric acid aerosols in the clouds and upper haze of Venus using Venus Express VAST and VeRa temperature profiles

Christopher D. Parkinson [a,*], Peter Gao [b], Rick Schulte [c], Stephen W. Bougher [a], Yuk L. Yung [b], Charles G. Bardeen [d], Valérie Wilquet [e], Ann Carine Vandaele [e], Arnaud Mahieux [e,g], Silvia Tellmann [f], Martin Pätzold [f]

[a] Department of Atmospheric, Oceanic, and Space Sciences, University of Michigan, Ann Arbor, MI 48109, USA
[b] Division of Geological and Planetary Sciences, California Institute of Technology, Pasadena, CA 91125, USA
[c] Santa Clara University, Santa Clara, CA 95053, USA
[d] National Center for Atmospheric Research, Boulder, CO 80307, USA
[e] IASB-BIRA, Brussels, Belgium
[f] Rheinisches Institut für Umweltforschung, Abteilung Planetenforschung, Cologne, Germany
[g] Fonds National de la Recherche Scientifique, rue d'Egmont 5, B-1000 Brussels, Belgium

ARTICLE INFO

Article history:
Received 15 March 2014
Received in revised form
8 November 2014
Accepted 27 January 2015
Available online 20 March 2015

Keywords:
Atmospheres composition
Atmospheres structure
Atmospheres dynamics
Venus
Venus atmosphere

ABSTRACT

Observations from Pioneer Venus and from SPICAV/SOIR aboard Venus Express (VEx) have shown the upper haze (UH) of Venus to be highly spatially and temporally variable, and populated by multiple particle size modes. Previous models of this system (e.g., Gao et al., 2014. Icarus 231, 83–98), using a typical temperature profile representative of the atmosphere (viz., equatorial VIRA profile), did not investigate the effect of temperature on the UH particle distributions. We show that the inclusion of latitude-dependent temperature profiles for both the morning and evening terminators of Venus helps to explain how the atmospheric aerosol distributions vary spatially. In this work we use temperature profiles obtained by two instruments onboard VEx, VeRa and SPICAV/SOIR, to represent the latitudinal temperature dependence. We find that there are no significant differences between results for the morning and evening terminators at any latitude and that the cloud base moves downwards as the latitude increases due to decreasing temperatures. The UH is not affected much by varying the temperature profiles; however, the haze does show some periodic differences, and is slightly thicker at the poles than at the equator. We also find that the sulphuric acid "rain" seen in previous models may be restricted to the equatorial regions of Venus, such that the particle size distribution is relatively stable at higher latitudes and at the poles.

1. Introduction

The sulphuric acid aerosols that make up the clouds and hazes of Venus play a crucial role in regulating the chemistry and radiation environment of the Venus atmosphere (Esposito et al., 1983; Mills et al., 2007). Conversely, variations in Venus' atmospheric conditions with latitude and longitude control the altitude and size distributions of the aerosol particles across the globe. This possible feedback leads to distinct structures in the clouds and hazes that vary from one location to another. For example, observations from Pioneer Venus using the Large Cloud Particle Size spectrometer (LCPS) have led to the discovery of multiple distinct cloud layers and multiple particle size modes in the equatorial region of Venus (Knollenberg and Hunten, 1980), as well as a decrease in haze optical thickness of an order of magnitude from the polar region to the lower latitudes. Temporal variations on the order of hundreds of days were also observed (Kawabata et al., 1980). Recent observations from Venus Express of the subpolar region (~60–70°N) have shown multiple particle modes in the UH (Wilquet et al., 2009), while a myriad of observations have revealed temporal variations with time scales on the order of Earth days (Linkin et al., 1986; McGouldrick and Toon, 2007; Markiewicz et al., 2007; Wilson et al., 2008, Barstow et al., 2012; Wilquet et al., 2012).

Interpretations of the observations using models that take into account both the detailed microphysics of cloud/haze formation and evolution and its variation with latitude and longitude have been lacking, with most of the modeling efforts focused on 1D atmospheric columns. However, the impact of these efforts should not be downplayed, as they are vital to our understanding of the local

* Corresponding author. Tel.: +1 626 818 9293.
E-mail address: theshire@umich.edu (C.D. Parkinson).

http://dx.doi.org/10.1016/j.pss.2015.01.023
0032-0633/

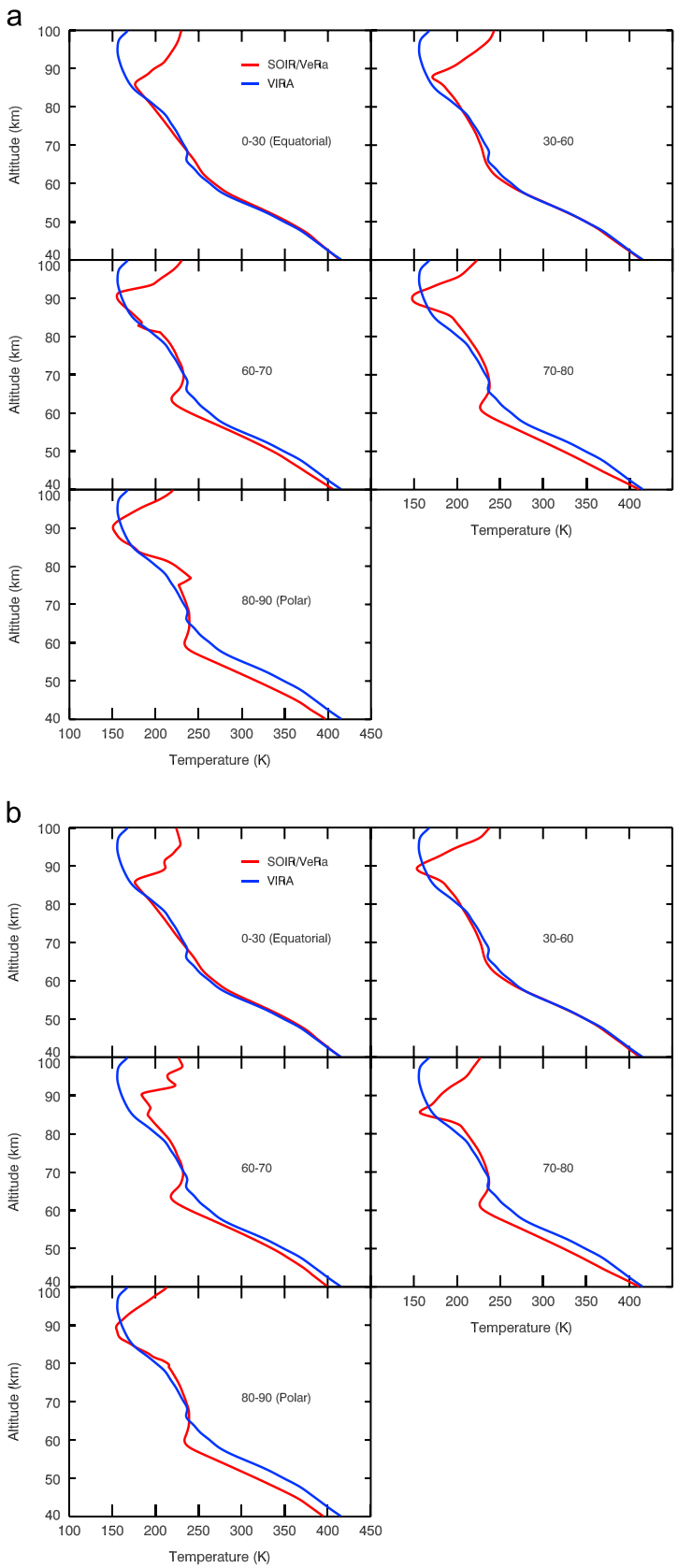

Fig. 1. (a) Retrieved SOIR VAST/VeRa (red) and VIRA (blue) temperature profiles at the Morning Terminator. The VIRA profiles are taken from the Venus International Reference Atmosphere (Seiff et al., 1985). (b). Same as (a), but for the Evening Terminator.

manifestation of the Venus clouds and hazes. The combined modeling work has shown that the highest sulphuric acid clouds are likely photochemical in nature, being the product of SO_2 photolysis and oxidation and nucleation onto cloud nuclei (Imamura and Hashimoto, 2001). The resulting cloud particles then sediment downwards and grow by condensation, turbulence, and coagulation (James et al., 1997; McGouldrick and Toon, 2007). These particles eventually reach a region of temperatures high enough for their evaporation back into sulphuric acid vapor, which are then transported upwards by diffusion. This results in their condensation onto cloud nuclei near the bottom of the clouds to form the lowest cloud layers (Krasnopolsky and Pollack, 1994). Separate from these modeling efforts are the works of Yamamoto and Tanaka (1998) and Yamamoto and Takahashi (2006), who did 3D-simulations of global atmospheric dynamics involving the clouds and hazes of Venus. While their results agreed with the observations satisfactorily, they did not tackle the details of nucleation in their treatment of aerosol microphysics.

The latest modeling attempt has been that of Gao et al. (2014), who used the Community Aerosol and Radiation Model for Atmospheres (CARMA) to simulate the combined clouds and UH system. They showed that the main cloud deck can be explained by photochemistry and condensational growth due to turbulence, while the UH variations may be due to transient upward winds lofting material from the clouds to the haze. Their model also featured a periodic oscillation in the particle sizes in the middle cloud – a turbulent region responsible for much of the condensational growth in the Venus clouds – and which they interpreted as a sulphuric acid "rain cycle". However, as with many previous modeling efforts, they did not consider how their aerosol distributions would change with variations in latitude, and whether the features they simulated would persist from equator to pole.

The SOIR instrument onboard Venus Express uses the solar occultation technique to sound the Venus atmosphere at its terminator. The density and temperature profiles are inferred from collected infrared SOIR transmittance spectra and the method has been described by Mahieux et al. (2012). The VAST (Venus Atmosphere from SOIR measurements at the Terminator) compilation initiated in that work has been improved. It is described in great detail in a companion paper in this issue (Mahieux et al., 2015). The updated VAST compilation is given on a specific latitudinal grid and differentiates between the morning and evening terminators. It confirms the main characteristics that were identified in the earlier version. In Mahieux et al. (2015), VAST is compared to temperature profiles obtained from other Venus Express instruments, VeRa and SPICAV/UV, and to ground based measurements, but we only concentrate on the comparison of VAST with the VeRa temperature profiles, which are relevant to the microphysical cloud modeling efforts of this paper owing to the range of altitudes needed and the domains of the temperature profiles retrieved by the two VEx instruments. This paper considers the latitude-dependent temperature profiles derived from the observations of the two VEx instruments, SOIR (through VAST) and VeRa and explains how we employ them in the current calculations and analysis. We also describe in detail how the inclusion of these latitude dependent temperature profiles improve the results of calculations carried out using the CARMA 3.0 model of Gao et al. (2014), in which only a single equatorial VIRA temperature profile was considered.

We provide a summary of Gao et al. (2014)'s Venus cloud and haze model and describe the VAST and VeRa temperature profiles in Section 2. In Section 3 we present the results of our simulations of the Venus clouds and hazes using the new temperature profiles, and we summarize our conclusions in Section 4.

2. Model

2.1. CARMA (The Community Aerosol and Radiation Model for Atmospheres)

CARMA is a 1D microphysical and vertical transport code that was originally created by Turco et al. (1979) to simulate Earth's stratospheric sulphate aerosols. It was later updated by Toon et al. (1988, 1989) to investigate the polar stratospheric clouds. Since then it has been upgraded several times by Jacobson and Turco (1994), Bardeen et al. (2008, 2011), and English et al. (2011) to include growth via coagulation and sulphate microphysics. McGouldrick and Toon (2007) used the model to simulate the condensation clouds of Venus, and Gao et al. (2014) extended this effort by modeling the clouds and the UH of Venus as a coupled system. We will use this latter model to quantify the effects that latitude-dependent temperature profiles have on the clouds and hazes of Venus. For brevity we refer the reader to Appendix A for a detailed description of the model used in this work, while providing a short summary below.

The nominal Venus cloud model of Gao et al. (2014) simulates a column of the Venus atmosphere from 40 to 100 km altitude and assumes production rate profiles of sulphuric acid and polysulphur condensation nuclei from Imamura and Hashimoto (2001), and meteoric dust from Kalashnikova et al. (2000). Toon et al. (1982) argued that photochemistry in the upper cloud region produces sulphur particles with masses comparable to observed mode 1 particles, while also suggesting that such particles act as condensation nuclei. The bottom boundary condition of Gao et al. (2014) consists of a fixed number density of mode 1 particles of radius $\sim$0.2 μm of 40 cm^{-3}, and a fixed sulphuric acid vapour mixing ratio of 3 ppm. Zero fluxes for all species are assumed for the top boundary condition.

The basic process of cloud formation and evolution in the model of Gao et al. (2014) is as follows: sulphuric acid is photochemically produced at $\sim$61 km altitude, and condenses on polysulphur condensation nuclei of radius 10 nm, which are also photochemically produced at the same altitude. This is consistent with the peak photochemical production of H_2SO_4 at 62 km from Mills and Allen (2007) and other early models. In Krasnopolsky (2012), it peaks at 66 km and the upward shift is caused by an unidentified NUV absorber that was neglected in the early models. In the UH, meteoric dust of radius 1.3 nm is assumed to form due to condensation of metallic vapour generated by the ablation of meteorites (Hunten et al., 1980), and which also act as condensation nuclei to any sulphuric acid in proximity. This initial population of (mode 1) sulphuric acid aerosols, with radius $\sim$0.2 μm then sediment downwards while growing by condensation and coagulation. Particles eventually reach the highly convective region at $\sim$53 km altitude, where intense turbulence – modeled using a large eddy diffusion coefficient – causes an increase in the growth rate of particles, thereby creating larger, 1 μm (mode 2) particles. These particles sediment further and coagulate with each other, forming still larger, $\sim$3 μm (mode 3) particles. Upon reaching the cloud base, these particles evaporate and deposit sulphuric acid in vapour form, which then diffuses upwards to mix with bare polysulphur condensation nuclei to create yet more cloud particles.

One major assumption of Gao et al. (2014) is a constant background water mixing ratio (see Fig. 3 of that paper). This was necessary, as CARMA cannot evaluate the exchange of water between the aerosol particles and the background water reservoir. Instead, they use a static water profile based on the models of Ignatiev et al. (1997) and the observations of Bertaux et al. (2007). However, Parkinson et al. (2015) (a companion paper in this issue) showed that the water content of the atmosphere above the cloud tops is closely controlled by the amount of SO_2 in the region, as both are removed by the formation of H_2SO_4. The abundances of SO_2 and H_2O are of the same order of magnitude, such that an excess of H_2O would result in the rapid removal of SO_2 and vice versa. Hence, SO_2 and H_2O can

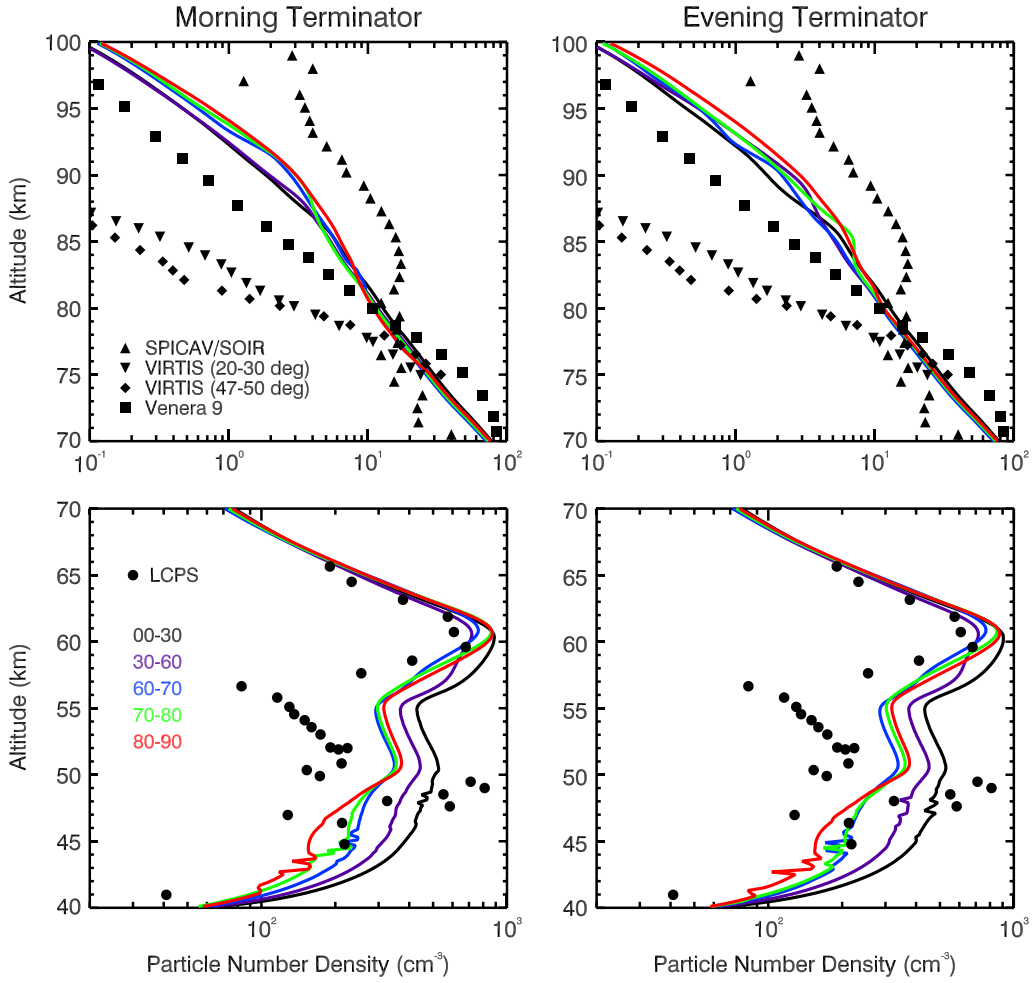

Fig. 2. Calculated number density of cloud and haze particles with radius $r > 0.115$ μm from our different latitude models compared to the total number density derived from LCPS (circles) (Knollenberg and Hunten, 1980), Venus Express SPICAV/SOIR (triangles) (Wilquet et al., 2009), Venus Express VIRTIS (upside down triangle: 20–30°N, diamond: 47–50°N) (de Kok et al., 2011), and Venera 9 (squares) (Krasnopolsky, 1983) observations for the MT (left) and ET (right) cases. The top two panels refer to the upper half of our model domain, while the lower two panels refer to the lower half of our model domain. Note the different × coordinates for the top and bottom panels.

regulate each other via formation of H_2SO_4 and the assumption of a fixed concentration may be false depending on local Venus atmospheric conditions. This is consistent with Krasnopolsky (2012), where it was found that the water content of the atmosphere could vary by an order of magnitude due to dynamics and variations of SO_2 above 70 km.

2.2. *Venus Express VAST and VeRa latitude dependent temperature profiles*

Fig. 1 shows the latitude-dependent temperature profiles used in this study. These differ from the fixed equatorial temperature profile used by Gao et al. (2014), which was derived from Seiff et al. (1985). However, fluctuations in the temperatures of the Venus upper mesosphere and lower thermosphere have been widely observed (Clancy and Muhleman, 1991; Bertaux et al., 2007; Mahieux et al., 2010, 2012, 2015; Tellmann et al., 2009, 2012), and thus the assumption of a fixed temperature profile is a simplification. In the current study, we use averaged temperature profiles from the SOIR's VAST compilation (Mahieux et al., 2015, Fig. 9) and individual, carefully chosen profiles from VeRa (Tellmann et al., 2009, 2012) to better reproduce the observed variability.

In Fig. 6 of Mahieux et al. (2015), VeRa profiles close to the terminator and VAST temperature profiles are compared in the 10 to 0.1 mbar region and the agreement is very good over the entire profile. VeRa temperature profiles depend on the upper boundary condition at an altitude of ~100 km and Mahieux et al. (2015) used VeRa profiles with an upper boundary condition of 200 K. We use very similar VeRa profiles here in this paper. However, in our case we did not use the VeRa profiles from Tellmann et al. (2009, 2012) above an altitude level of ~85 km (1 mbar level). We should further point out that there is reasonable correspondence between the Venus Thermospheric General Circulation Model (VTGCM) modeling and VAST temperatures (see Bougher et al., 2015, a companion paper in this issue).

The Venus Express Radio Science Experiment (VeRa) uses two coherent radio frequencies at X-band (8.4 GHz) and S-band (2.3 GHz) to sound the atmosphere and ionosphere in Earth occultation geometry (Häusler et al., 2006, 2007). More than 700 vertical profiles of electron density in the ionosphere (Peter et al., 2014), and neutral number density, pressure, and temperature in the middle atmosphere of Venus have been retrieved so far (Pätzold et al., 2007; Tellmann et al., 2009, 2012). Radio attenuation measurements are also used to retrieve absorptivity profiles of sulphuric acid in the Venus cloud deck (Oschlisniok et al., 2012). The atmospheric profiles cover the upper troposphere and mesosphere of the planet between altitudes of ~40 to 90 km with a high vertical resolution of only a few hundred meters. The measurement uncertainty is highest at the top of the profiles (~10% at 100 km) where an upper boundary condition has to be implemented. The measurement uncertainty decreases with decreasing

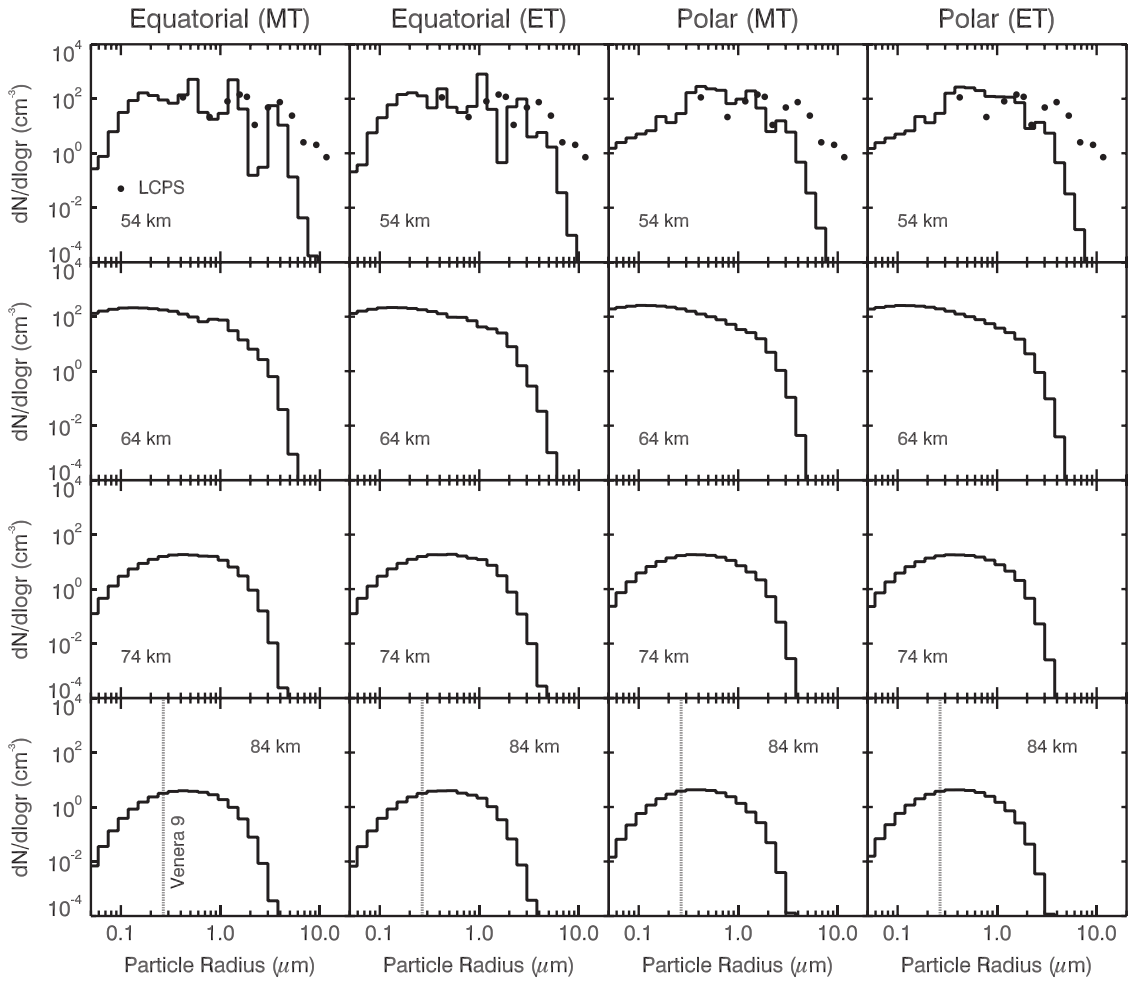

Fig. 3. Calculated particle size distributions at various altitudes for the MT and ET cases of the equatorial (0–30°) and polar (80–90°) nominal models. LCPS size data at 54.2 km (dots) (Knollenberg and Hunten, 1980) and the average particle radius derived from Venera 9 data at 84 km (Krasnopolsky, 1983) are plotted for comparison.

altitude, reaching a fraction of a Kelvin at the lower boundary of the profile. A nearly uniform coverage in the southern hemisphere is achieved due to the highly elliptical orbit of Venus Express while atmospheric profiles in the northern hemisphere are more clustered around the high northern latitudes covering almost all local times. A detailed description of the instrument can be found in Häusler et al. (2006, 2007).

Following directly from Mahieux et al. (2015), the 150 K isotherm above the cold layer shows a latitude dependence on the morning side only, varying between 3×10^{-6} mbar (approx. 133 km) at the equator and 10^{-6} mbar at the poles (approx. 138 km). Below, in the region of interest relevant for this paper, a warm layer is observed at about 100–110 km, with temperatures around 220 K, and is similar at both morning and evening terminators. It is nearly constant for latitudes lower than 80°, and reaches colder values when approaching the poles (between 180 and 200 K). This warm layer is partially due to transport (heat advection) from the warm dayside (i.e. this terminator warm layer is connected to the warm dayside layer at ~115 km at noon). We refer the reader to Bougher et al. (2015) for more details. Alternatively, these warm temperatures could be due to the presence of aerosols in the UH layer, to which SOIR is not sensitive (Bougher et al., 2015; Mahieux et al., 2015; Wilquet et al., 2012). At the morning terminator, a cold layer is observed in the 80 km region, presenting a clear latitudinal dependence, with temperatures gradually increasing from 140 K at the poles to 180 K at the equator. The latitudinal dependence is clearly seen on the 190 K isotherm, varying between 0.25 mbar (approx. 90 km) at the Equator and 0.016 mbar (approx. 100 km). On the contrary, at the evening terminator, two minima are observed down to temperatures of 160 K, one at the poles and one at mid-latitude. The 190 K isotherm also shows a stronger latitude dependency. We refer the reader to the comprehensive comparison between the VTGCM simulated and SOIR observed temperature profiles (~70–160 km) given in the companion paper Bougher et al. (2015).

For each latitude bin in each of the plots shown in Fig. 1, we connected the VAST and VeRa temperature profiles at the 1 mbar level (~85 km) and smoothed the entire profile using a 1 km "moving average" cubic spline. Thus, for a given altitude level, the temperature is the average of all data points within 1 km. These profiles were then interpolated from 40 km to 100 km (the CARMA range) to match the altitude grid used by Gao et al. (2014) in their paper for computational purposes.

3. Results and discussion

Fig. 2 shows the model number densities computed using the VAST and VeRa temperature profiles as compared to available LCPS (Knollenberg and Hunten, 1980), SPICAV/SOIR (Wilquet et al., 2009), VEx VIRTIS (de Kok et al., 2011), and Venera 9 data (Krasnopolsky, 1983) for each of the 5 latitude bins. The agreement between model and data is satisfactory for all of our number density profiles, especially when taking into account the scatter

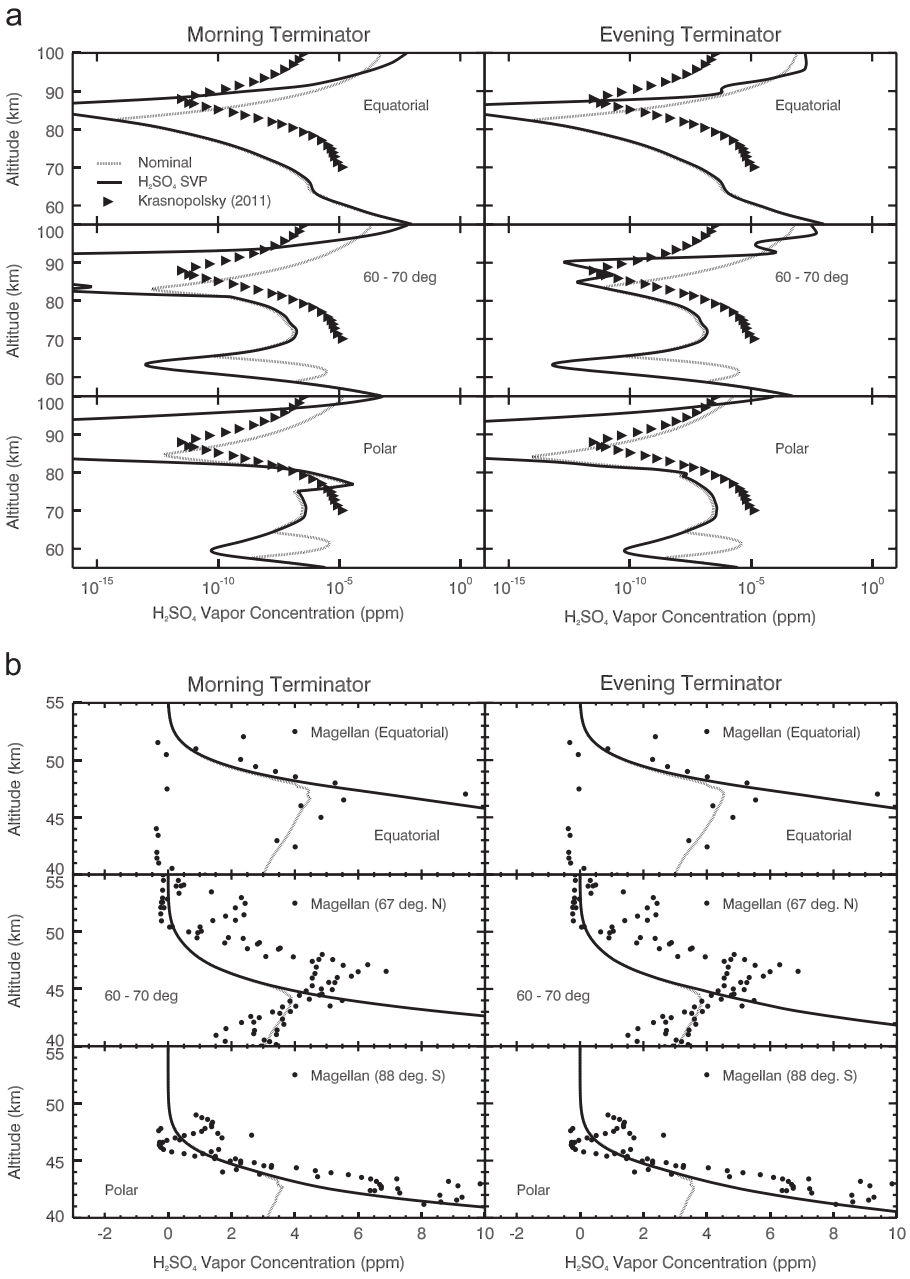

Fig. 4. (a) Calculated sulphuric acid vapour mixing ratios (gray) from 55 to 100 km in the equatorial (top), 60–70° (middle), and polar (bottom) regions at the MT (left) and ET (right), compared with the sulphuric acid saturation vapour mixing ratio (black) and the results of Krasnopolsky (2011) (triangles) derived from Venus Express observations. (b) Calculated sulphuric acid vapour mixing ratios (gray) from 40 to 55 km in the equatorial (top), 60–70 (middle), and polar (bottom) regions at the morning (left) and evening (right) terminators, compared with the sulphuric acid saturation vapour mixing ratio (black) and Mariner 10 and Magellan radio occultation data analyzed by Kolodner and Steffes (1998) (circles).

between the different data sets. Despite this agreement, it is clear that the cloud distribution is variable between the latitudinal regions, even when the temperature variations applied are relatively small. Differences between the morning terminator and evening terminator (MT and ET, respectively) are minimal.

Fig. 3 shows the size distributions of the cloud and haze particles at various altitudes for the MT and ET cases, corresponding to temperature profiles from each of the two extreme latitude cases, viz., the polar (80–90°) and equatorial (0–30°) regions. The results clearly point to a distinct behavior at lower altitude between the equator and the polar regions. For the equatorial case, three distinct peaks exist in the size distributions, corresponding to the three size modes as observed by Pioneer Venus (Knollenberg and Hunten, 1980). In contrast, the polar case shows very little distinction between the size modes, with mode 1 particles dominating. Again, the MT and ET cases show little difference between them.

Our model predicts a mono-modal size distribution for all cases in the UH, suggesting that this is the steady state distribution for all latitudes. The particle radius corresponding to the peak in the size distribution at 84 km is in good agreement with the results of Venera 9 (Krasnopolsky, 1983), though they all appear to be larger by ~30%. This may indicate that our eddy diffusion coefficient at this altitude is too large, thereby bringing up into the UH cloud particles that are larger than what is actually there. The alternative explanation is the addition of meteoric dust into the model, though that is unlikely given their relative insignificance on long time scales (Gao et al., 2014). Meanwhile, the number density

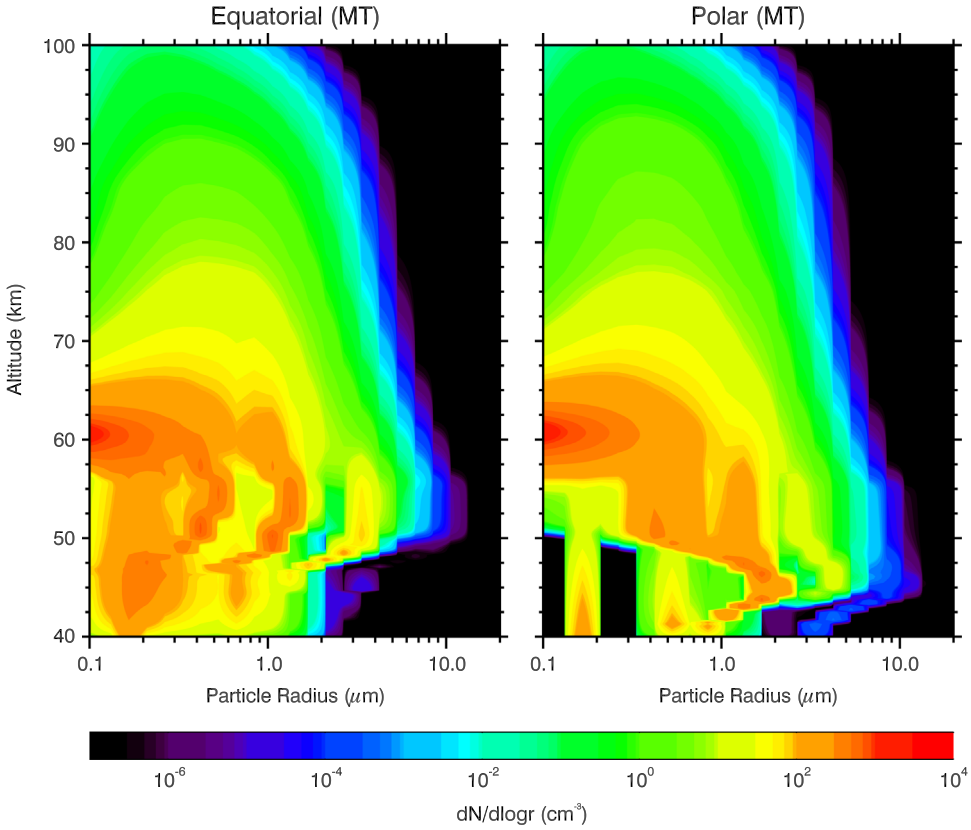

Fig. 5. Calculated particle number density as a function of particle size and altitude for the equatorial MT (left) and polar MT (right).

(Fig. 2, upper panels) profiles of the UH are similar for all our latitude cases, with maximum difference between them of no more than a factor of 2. These profiles also lie between the observations of Wilquet et al. (2009), de Kok et al. (2011), and Krasnopolsky (1983), which reinforces the observed variability of the UH, as well as the conclusions of Gao et al. (2014), who suggested that transient events play a major role in shaping the UH and that it is rarely in steady state (see Appendix A).

Fig. 4 shows a comparison between the predicted mixing ratios of sulphuric acid vapour in the equatorial, 60–70°, and polar regions at the MT and ET and the observed mixing ratio from Mariner 10 and Magellan radio occultation data as analyzed by Kolodner and Steffes (1998) and the calculated mixing ratio from Krasnopolsky (2011), who used Venus Express data. Our model results show a satisfactory fit to the Mariner 10 data points for the equatorial case, with a cloud base at ~48 km. For the 60–70° case, the saturation vapor pressure curve within the model is a bit too low when compared with the Magellan radio occultation analysis, but match much better below the cloud base, which is at ~45 km in this case. The 80–90° case has the right saturation vapor pressure curve, but too little gas below the clouds—we attribute this to the fixed 3 ppm sulphuric acid vapour bottom boundary condition limiting the curve above it to around that value. It is likely then that this bottom boundary condition is not universal between the different latitudes. The cloud base for the polar case is at ~43 km. In the UH, the fit between our results and that of Krasnopolsky (2011) is the best at high latitudes. This is expected, as they used high latitude Venus Express data in their calculations. The lack of significant differences between the MT and ET cases continue here, and thus all subsequent results will only include the MT cases.

That the equatorial and polar model saturation vapor pressure curves agree so well with the Mariner 10 and Magellan radio occultation data provides great confidence regarding the temperature profiles for these regions. In contrast, the 60–70° region had the fewest SOIR measurements at the ET and MT, thus resulting in lower statistical confidence. This could be the cause of the poorer agreement between simulation and observations at these latitudes.

For the equatorial and polar regions the results shown in Fig. 4 also agree with the sulphuric acid vapor abundance derived from VeRa observations between 2006 and 2011 in the southern hemisphere. The 122 zonal and temporal averaged sulphuric acid vapour profiles in Oschlisniok et al. (2012) peak around the cloud base (~50 km), showing maximal equatorial abundances of ~3–5 ppm and maximal polar abundances of ~0–1 ppm.

Two major regions of supersaturation occur in the results shown in Fig. 4. The supersaturation at 61 km is attributable to the production of sulphuric acid vapour there. The cause of the supersaturated (and unsaturated) regions above 80 km is less clear, though the shape of the sulphuric acid mixing ratio curve is consistent with the results of Krasnopolsky (2011) in the polar region. As previously mentioned, transport dominates over the microphysics in this region, and thus the supersaturations could be due to eddy diffusion reducing the actual sulphuric acid vapour mixing ratio gradient as compared to the saturation vapour pressure curves, which tend to have steeper gradients above 80 km. The shape of the mixing ratio curves is thus a balance between eddy diffusion and the condensation/evaporation rates of the particles in the supersaturated/unsaturated regions, respectively.

Fig. 5 shows number density as a function of both altitude and particle radius for our two extreme latitude cases. The equatorial case is very similar to Fig. 11 in Gao et al. (2014) with one notable difference: there is a two to four orders of magnitude increase in nominal particle density in small pockets for particles greater than 2 μm (mode 3) between 45 and 55 km for our model calculations. This is an indicator that the "rain cycle" found in the results of Gao et al. (2014) is also in our equatorial case (see Appendix A and discussions below), as these pockets were seen in that study to be transient populations that quickly sedimented out of the middle

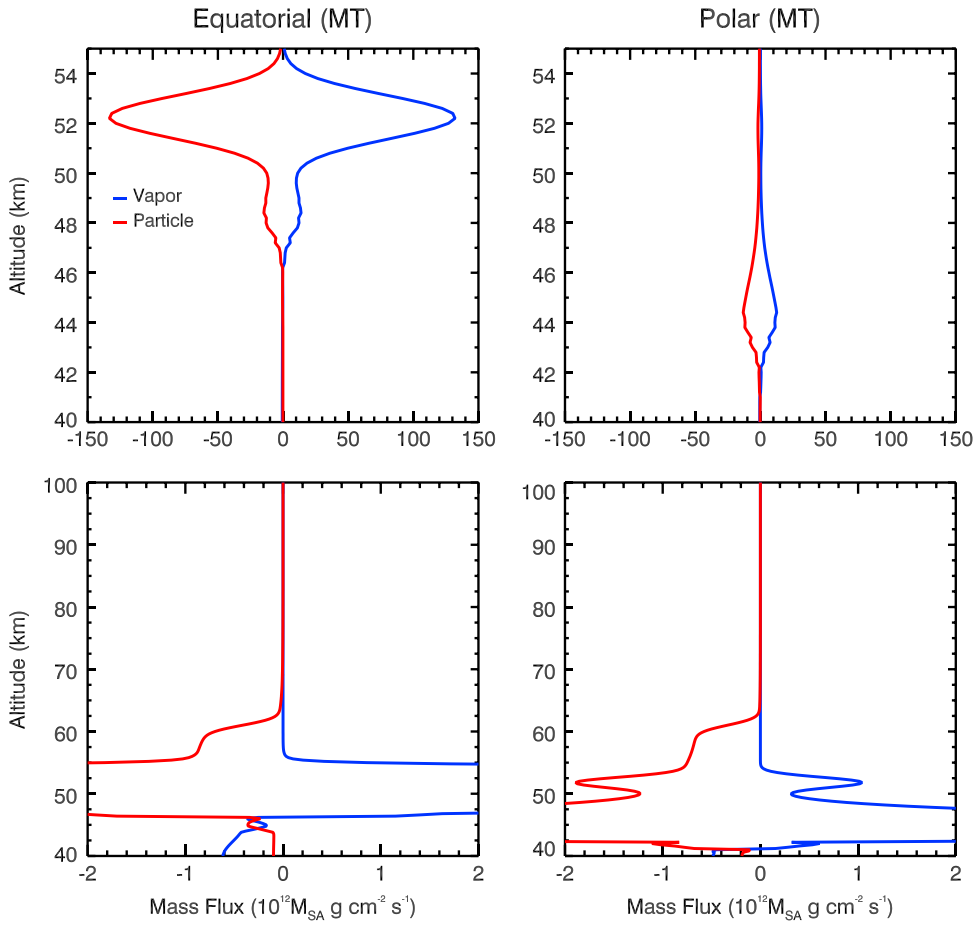

Fig. 6. Calculated equatorial MT (left) and polar MT (right) sulphuric acid vapour (blue) and particle (red) mass fluxes in units of 10^{12} M_{SA} per unit area per second, where M_{SA} is the mass of a single sulphuric acid molecule $\sim 1.6 \times 10^{-22}$ g. Note the different axes coordinates between the top and bottom panels: the top panel shows the high flux values of the middle cloud, while the bottom panel shows the lower flux values at the other altitudes (but which also includes the middle cloud).

cloud. The polar case, in contrast, shows none of the activity of the equatorial case with slow or little growth beyond mode 2 in the cloud deck, as well as no evidence of precipitation of any kind. Furthermore, the lone mode 1 particle number density peak in the lower altitudes for the polar case indicates that our assumption of a fixed mode 1 size and number density bottom boundary condition is likely false for this region of the atmosphere, as that peak is likely due to the boundary condition itself rather than arising naturally from cloud processes. Clearly, sensitivity studies of the bottom boundary condition for these higher latitudes are necessary to more realistically simulate the cloud distributions there. The polar case also showcases a mode 2 peak starting at much lower altitudes than in the equatorial case, consistent with the slower condensation and coagulation time scales associated with the lower temperatures. On the other hand, a larger mode 3 particle size results near the cloud base, since the particles have more time to sediment and grow due to the lower cloud base. Readers interested in obtaining a time evolution sequence of these plots may obtain the data movies from the lead author by emailing him.

Fig. 6 shows the mass flux of sulphuric acid vapour and cloud/haze particles for the equatorial (left) and polar (right) MT cases. The differences between them are striking, especially in the middle and lower clouds (top). The middle cloud fluxes, for example, are much greater in the equatorial case than the polar case; this is consistent with the difference in mass loading between the equatorial and polar middle clouds (see Fig. 2). In contrast, while the lower cloud fluxes for the polar case is shifted down from that of the equatorial case, likely due to the lower cloud base, their magnitudes are similar. This is due to the similar sulphuric acid mixing ratios at the cloud base between the two cases (see Fig. 4). The fluxes for the other altitudes (bottom) are fairly similar, though again the polar case has lower fluxes in the upper cloud, and a cloud base much closer to the bottom of our model domain.

Figs. 7 and 8 show the time evolution of the particle size distribution at various altitudes for the Equatorial and Polar cases, respectively. For the equatorial region, there exist quasi-periodic variations above the clouds and in the upper cloud that are very small. In contrast, the middle cloud shows quasi-periodicity on a time scale of $\sim$3 Earth months with changes in particle number density of several orders of magnitude. *This phenomenon does not seem to be occurring at all in the polar region, where temperatures are lower than in the clouds*. We refer the reader to Appendix A for a possible mechanism for this quasi-periodic variability. In essence, the lower temperatures of the higher latitudes impede both condensational and coagulational growth, which are essential to the occurrence and time scales of this process.

Minor differences in the particle size evolution exist between the MT and ET in the UH (not shown), though they are unlikely to be significant and are probably random fluctuations in the model evolution. They are not a diurnal effect as the time scales in the oscillations are on the order of months rather than “days”, and diurnal solar forcing is not included in the model.

The above results illuminate the effect of the latitudinally dependent temperature profiles on the clouds and UH of Venus. The primary effect of changing the temperature on the clouds and hazes are the alterations to the condensation and coagulation time scales

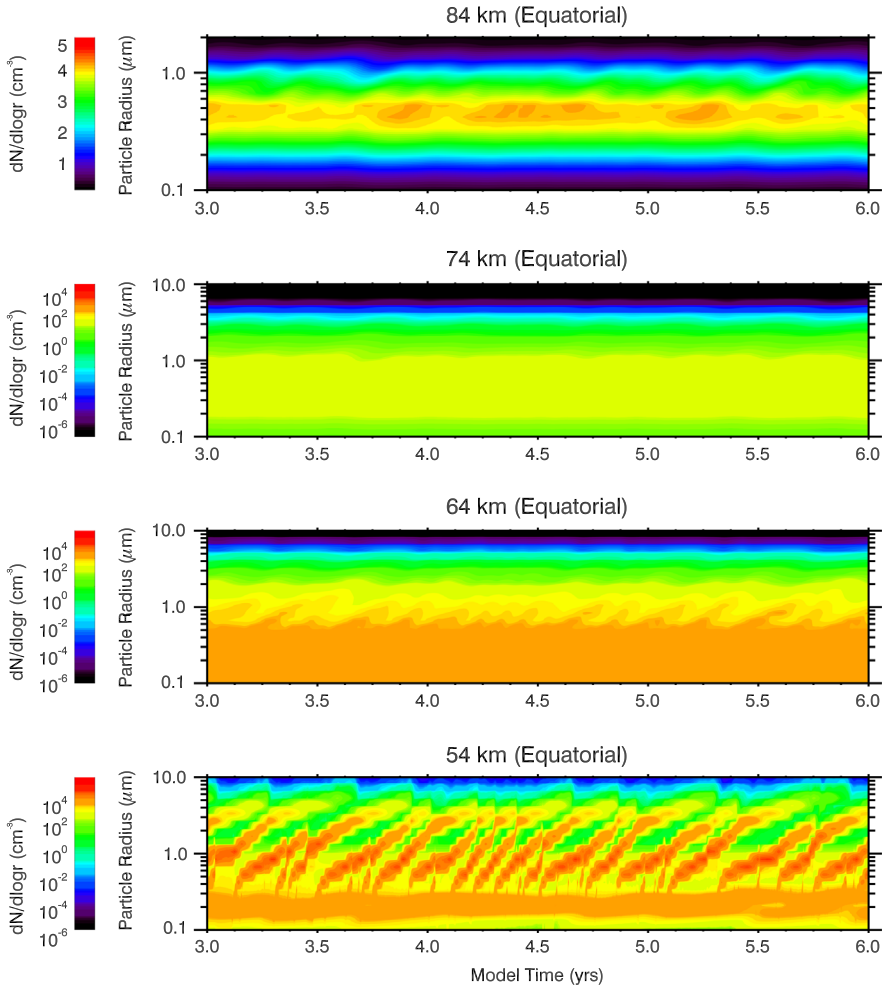

Fig. 7. Time evolution of the calculated particle size distribution at 84, 74, 64, and 54 km altitude from $t=3$ Earth years to $t=6$ Earth years for the Equatorial MT case. Note the different number density contour and y axis scale for the 84 km plot.

(see the Appendix of Toon et al., 1989). The cooler temperatures in the higher latitude regions result in less condensation, and thus smaller particles. Fig. 2, which plots only particles with radius >0.115 μm, shows clearly how the >0.115 μm particle number density of the clouds (bottom) generally decrease with increasing latitude. This trend stalls for the upper and middle clouds of latitudes higher than 60° due to the slower sedimentation of smaller particles. As a result, the higher latitudes will have a greater number density of particles near the production site at 61 km since it takes longer for the smaller particles there to fall into the lower cloud; this is shown in Fig. 3, which features a factor of 1.5–2 higher small particle ($r\sim0.1$–0.2 μm) number density in the size distribution at 64 km for the polar case than for the equatorial case. The lower mass loading for higher latitudes is also seen in Fig. 6 in the form of lower mass fluxes, as described earlier. The slower condensation and coagulation also lead to a diminutive or nonexistent quasi-periodic oscillation in the middle cloud particle sizes as compared to the results of Gao et al. (2014) and the equatorial cases of the present work.

In contrast to the clouds, the UH is mostly unaffected. This is due to the already low temperatures of the region, such that the temperature differences between the latitudes make little difference to the microphysics. For these low temperatures, the condensation and coagulation times scales are much longer than the transport time scale due to eddy diffusion, and thus the UH particle distribution is mostly the result of transport. This is apparent in the shape of the steady state number density curves in Fig. 2, which are linear in log space, consistent with a well-mixed state.

In order to generate mode 2 haze particles using the single equatorial VIRA temperature profile, Gao et al (2014) required the effects of transient winds (see Appendix A). We do not consider winds in this work, though we plan to include updrafts/downdrafts by incorporating more realistic winds calculated from the Michigan VTGCM (e.g. Bougher et al., 2006; Brecht et al., 2011), along with the updated SOIR/VeRa temperature profiles shown here and discussed in greater detail in the companion papers in this issue (cf. Bougher et al., 2015; Mahieux et al., 2015; Parkinson et al., 2015). Complimenting the VTGCM wind results are the observations of the Vega balloons, which acquired vertical speed and acceleration information during their mission (Linkin et al., 1986). These observations have been further interpreted by modeling (e.g. Gao et al., 2014) and the updrafts/downdrafts from the VTGCM will be chosen such that they are consistent with these efforts.

4. Summary and conclusions

In this study we simulated the clouds and upper haze of Venus using version 3.0 of the microphysical and vertical transport model CARMA in combination with the Venus Express VAST (from SPICAV/SOIR) and VeRa latitudinally dependent temperature profiles. We have shown that there are minimal differences between

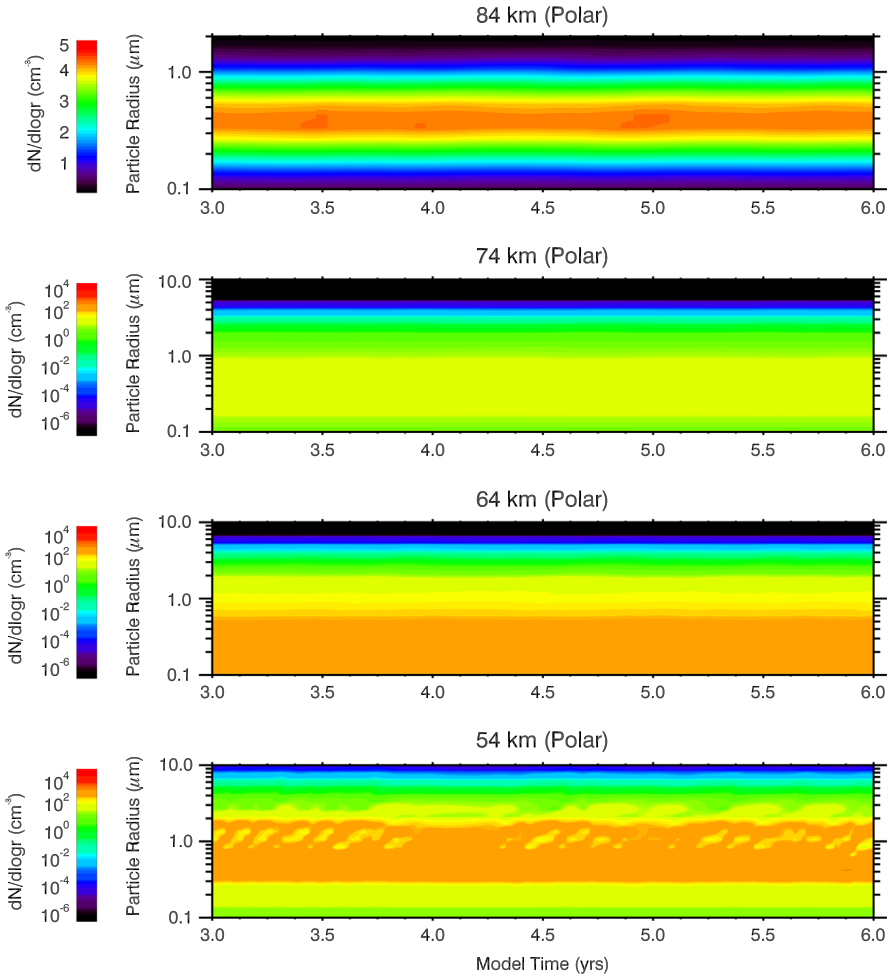

Fig. 8. Same as Fig. 7, but for the Polar MT case.

the morning and evening terminator cloud/haze distributions. There are also relatively minimal differences in the UH for the range of latitudes examined, with the implication that the UH is not affected by our range of observed temperature profiles due to the already low temperatures of the region allowing transport to dominate over condensation and coagulation. In contrast, large differences are obtained in the cloud deck between the equatorial and polar regions, illustrating the relative similarly between the condensation/coagulation and transport time scales. The quasi-periodic variability in our equatorial modeling results has a period of ~3 Earth months and is most apparent in the middle cloud deck. *This process does not occur for the polar region*, and thus is likely very dependent on temperature.

In this work we do not change the background water content, the bottom boundary conditions, the eddy diffusion coefficient, or include changes in the wave drag forcing (as input from the VTGCM). Our future work will examine the impacts of including all these tunable parameters in the photochemical and dynamical modeling.

Acknowledgements

Venus Express is a planetary mission from the European Space Agency (ESA). We wish to thank all ESA members who participated in the mission, in particular, H. Svedhem and D. Titov.

We thank our collaborators at IASB-BIRA (Belgium), Latmos (France), and IKI (Russia). We thank CNES, CNRS, Roskosmos, and the Russian Academy of Science. The research program was supported by the Belgian Federal Science Policy Office and the European Space Agency (ESA, PRODEX program, contracts C 90268, 90113, and 17645). We acknowledge the support of the "Interuniversity Attraction Poles" programme financed by the Belgian government (Planet TOPERS). The research leading to these results has received funding from the European Union Seventh Framework Program (FP7/2007-2013) under grant agreement no. 606798. A. Mahieux thanks the FNRS for the position of "chargé de recherche".

VeRa is partially funded by the Deutsches Zentrum für Luft- und Raumfahrt (DLR) unter Contract 50 QM 1004.

The contribution of Bougher was funded in part by subcontract no. B99073JD to Southwest Research Institute.

Appendix A. The CARMA model

Gao et al. (2014) investigates the Venus clouds and upper haze (UH) as a coupled system, using version 3.0 of CARMA (Community Aerosol and Radiation Model for Atmospheres) (Bardeen et al., 2008, 2011). While the core of the model is essentially the same as those described in the previous works, as cited in Section 2.1 of the present text, specific details are added in order to solve the Venus cloud/UH problem.

The model assumes the equatorial VIRA temperature/pressure profile derived by Seiff et al. (1985). The eddy diffusion coefficient profile is constructed empirically from that of Imamura and Hashimoto (2001) (40–70 km) and Krasnopolsky and Parshev (1983) (70–100 km). A constant-flux wind profile is used in a separate set of transient wind

tests that extends from 40 km to 70 km, above which the wind speed tapers to zero linearly at 75 km. The maximum amplitude of this wind is 1 m s^{-1} at 70 km. The three profiles in the nominal (no wind) model are fixed during the model runs and no feedbacks between the clouds/hazes and the temperature/pressure/eddy diffusion coefficient profiles are calculated.

The photochemical production of sulphuric acid and sulphur is assumed to proceed via the pathway

$$3SO_2 + 2H_2O \rightarrow S + 2H_2SO_4 \quad (A.1)$$

(Yung and DeMore, 1982; Krasnopolsky and Parshev, 1983). However, depending on the local abundance of O_2, the alternate chemical pathway

$$SO_2 + (1/2)O_2 + H_2O \rightarrow H_2SO_4 \quad (A.2)$$

can dominate. Thus the actual production rate of S is uncertain, and therefore so are the production rates of Sx (polysulphur) and Sx CNs. For their nominal model, Gao et al. (2014) use reaction A.1 along with the production profiles of Imamura and Hashimoto (2001), though they do test the effect of decreasing the polysulphur CN production.

The size of the CN is also uncertain since there are no direct measurements that distinguish cloud particles from CNs. Gao et al. (2014) assume the size to be 10 nm. This value is a compromise between assuming a molecular CN on the order of ~0.2 nm (Bardeen et al., 2011), and a mode 1 CN with radii ~0.2 μm (Imamura and Hashimoto, 2001). The compromise arises from the assumption that there exists finite time between the first nucleation of the CN from polysulphur vapor and the build up of sulphuric acid to saturation levels defined by the curved surface of the growing polysulphur CN, as polysulphur has a much lower saturation vapor pressure than sulphuric acid (Lyons, 2008). If the time between these two events were short, then the CN would still be small when sulphuric acid begins nucleating on it, and vice versa. This time scale can be calculated by correctly treating both sulphur and sulphuric acid microphysics, but this is beyond the scope of Gao et al. (2014) as well as the present study.

As summarized in the present text, the modeled process involves the photochemically produced sulphuric acid condensing onto polysulphur CNs, with the resulting particles transported upwards and downwards by diffusion and sedimentation. Growth of the particles by condensation and coagulation occurs in the middle and lower clouds due to turbulence, with evaporation of particles below the cloud decks. The calculated steady state results agree with the observations satisfactorily, especially when the measured variability of the Venus clouds/hazes are considered. Fig. A.1 shows the particle number density as a function of particle radius and altitude in steady state, illustrating the multiple size modes and their distribution with height. In addition to these results, Gao et al. (2014) also considered the effects of decreasing the production rate of CNs and the application of transient winds, and found a quasi-periodic oscillation in the particle sizes of the middle cloud that seem to suggest precipitation. We will discuss these results in more detail below.

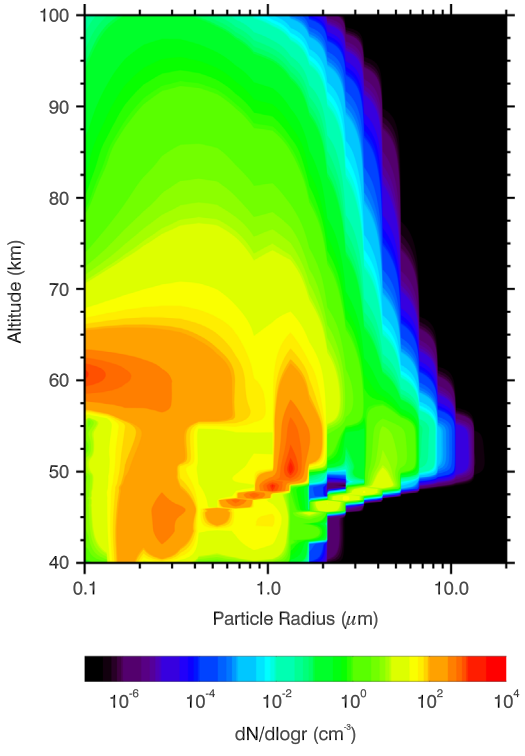

Fig. A.1. The calculated particle number density of the Venus clouds and upper haze as a function of particle radius and altitude for the nominal case of Gao et al. (2014). Reprinted from Gao et al. (2014) with permission.

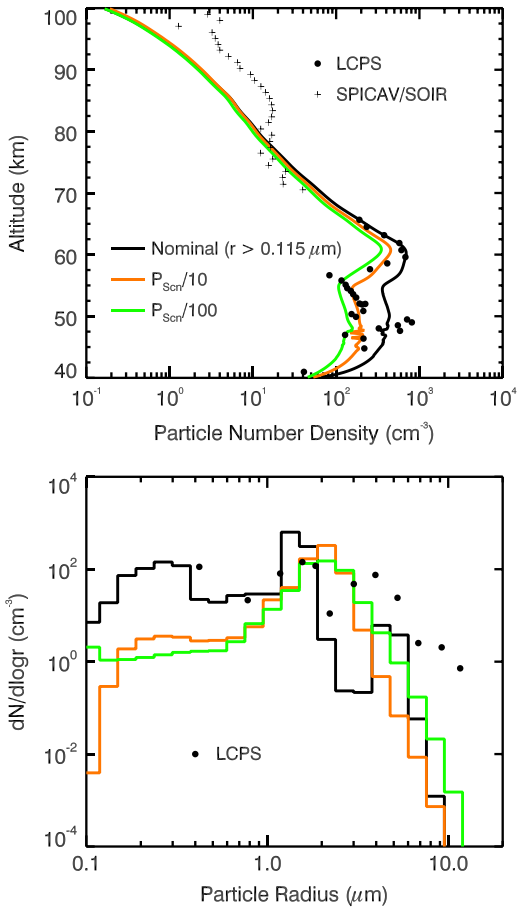

Fig. A.2. The calculated number density of particles with $r > 0.115$ μm (top) and particle size distribution (bottom) at 54 km altitude. The nominal model is plotted in black; the model with an order of magnitude decrease in the condensation nuclei production rate P_{Scn} is plotted in orange; and the model with two orders of magnitude decrease in P_{Scn} is plotted in green. The particle number density and size distribution (at 54 km) data from LCPS (dots) (Knollenberg and Hunten, 1980) and the particle number density data from Venus Express SPICAV/SOIR (pluses) (Wilquet et al., 2009) are plotted for comparison. Reprinted from Gao et al. (2014) with permission.

Varying the condensation nuclei production rate

The production rate of polysulphur CNs is uncertain due to the different chemical pathways that lead to generating sulphuric acid and how they depend on the local oxygen content. In response, Gao et al. (2014) tested cases where the polysulphur CN production rate is decreased by one and two orders of magnitude. The resulting particle number density and size distributions (at 54 km) are plotted in Fig. A.2, which shows that the particle number density decreases with decreasing polysulphur CN production. This is expected, since the fewer CNs there are, the fewer and larger the resulting cloud particles, as the same amount of sulphuric acid is being shared across fewer CNs. This is reflected in the size distribution, which moves to larger radii with decreasing sulphur CN production. In fact, since there is more sulphuric acid for a given CN, the mode 1 particles have essentially all grown into mode 2 particles in the lower CN production cases. The lack of a distinct mode 3 may be due to the low rate of coagulation caused by the lower particle number density. In comparison with data, the case with the one order of magnitude decrease in polysulphur CN production seem to best fit the observed particle number density, though none of the models fit the high particle number density of the lower cloud, and neither of the low polysulphur CN production cases fit the size distribution data.

Quasi-periodic variations in the middle cloud

Gao et al. (2014) found in their nominal model results a quasi-periodic oscillation with period ~6 months in the size distribution of the middle cloud despite fixed atmospheric conditions. Fig. A.3 shows the time evolution of the particle radii at four altitudes across the model domain during the latter half of the simulation, when the model has reached "steady" state. The oscillation manifests as the repeated growth and fallout of particles, i.e. mode 1 particles of radii ~0.2 μm quickly grow into larger mode 2 particles of radii ~1 μm at almost random times; the mode 2 particles then remain stable, or grow very slowly for the aforementioned period of ~6 months before becoming mode 3 particles of radii ~3 μm, which then sediment quickly into lower altitudes. Gao et al. (2014) attributes the cycle to coagulation of mode 1 particles leading to growth that allows the resulting particles to cross the Kelvin barrier at lower altitudes than the main production site at 61 km; these "growth pulses" then lead to the mode 2 particles, which coagulate further to form mode 3 particles.

There is currently no observational evidence for this cycle or the processes that cause it. However, tantalizing hints of periodic changes in the middle and lower clouds have been observed by McGouldrick et al. (2011) that have periods of roughly ~6 months, though it appears to be restricted to the mid-latitudes.

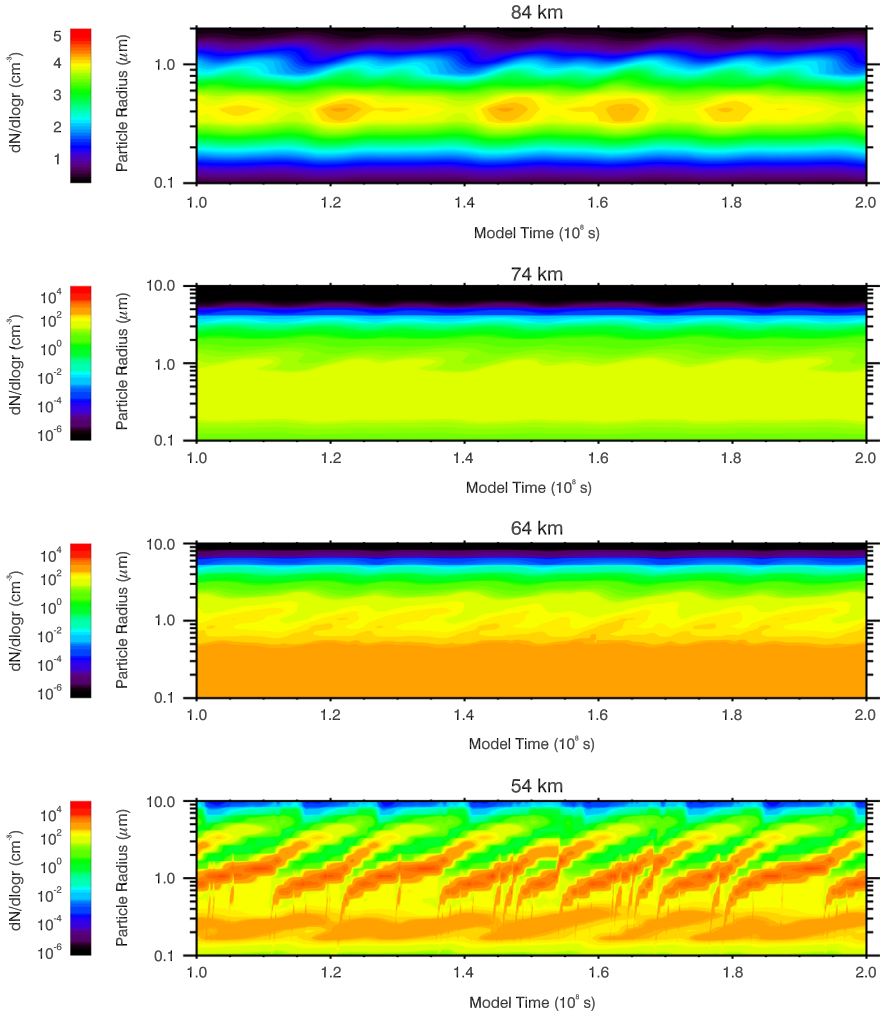

Fig. A.3. Time evolution of the particle size distribution at 84, 74, 64, and 54 km altitude. Note the different number density contour and *y*-axis scales for the 84 km plot. Reprinted from Gao et al. (2014) with permission.

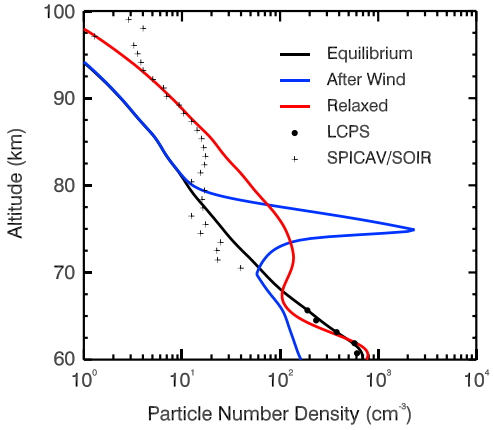

Fig. A.4. Calculated particle number density profiles of the upper haze before (black), immediately after (blue) and ~6 Earth days after (red) a ~14 h transient wind event. The number density data from LCPS (dots) (Knollenberg and Hunten, 1980) and Venus Express SPICAV/SOIR (pluses) (Wilquet et al., 2009) are plotted for comparison. Reprinted from Gao et al. (2014) with permission.

Transient winds

Gao et al. (2014) use transient wind gusts at the cloud tops to attempt to explain the bimodal particle size distribution observed by Wilquet et al. (2009) in the UH, with the assumption that the larger particles observed were upwelled into the UH by the gusts. Fig. A.4 shows the effect a 14 h gust has on the UH particle number density and its subsequent evolution with time. Immediately after the gust, a detached haze layer forms above the altitude where the wind profile drops to zero. The location of the detached layer is dependent on the location of the wind cut off and is thus artificial, but the existence of the detached haze in the first place should not depend on where the wind cut off is, as long as the vertical wind eventually overturns at some altitude. Over the next few Earth days, the haze layer diffuses both upwards and downwards, resulting in a particle number density profile in good agreement with the observations of Wilquet et al. (2009) above 85 km.

The major issue regarding these tests is the intensity and duration of the gusts. Gao et al. (2014) argued that a 14-h gust could be possible if it arose from intensified convection in the middle cloud at the subsolar point generating gravity waves in the upper cloud, which can potentially last for several hours. Thus, the structures seen in the UH may at least partly be due to transient events such as cloud top winds.

References

Bardeen, C.G., Toon, O.B., Jensen, E.J., Marsh, D.R., Harvey, V.L., 2008. Numerical simulations of the three dimensional distribution of meteoric dust in the mesosphere and upper stratosphere. J. Geophys. Res. 113 (D17202), 15.

Bardeen C.G., Conley A., Jensen E., Colarco P., Toon O., Fan T., Smith J., 2011. The CARMA 3.0 Microphysics Package in CESM. In: Whole Atmosphere Working Group Meeting.

Barstow, J.K., Tsang, C.C.C., Wilson, C.F., Irwin, P.G.J., Taylor, F.W., McGouldrick, K., Drossart, P., Piccioni, G., Tellmann, S., 2012. Models of the global cloud structure on Venus derived from Venus Express observations. Icarus 217, 542–560.

Bertaux, J.-L., Vandaele, A.-C., Korablev, O., Villard, E., Fedorova, A., Fussen, D., Quemerais, E., Belyaev, D., Mahieux, A., Montmessin, F., Muller, C., Neefs, E., Nevejans, D., Wilquet, V., Dubois, J.P., Hauchecorne, A., Stepanov, A., Vinogradov, I., Rodin, A., the SPICAV/SOIR team, 2007. A warm layer in Venus' cryosphere and high-altitude measurements of HF, HCl, H_2O, and HDO. Nature 450, 646–649.

Bougher, S.W., Rafkin, S., Drossart, P., 2006. Dynamics of the Venus upper atmosphere: outstanding problems and new constraints expected from Venus Express. Planet. Space Sci. 54, 1371–1380. http://dx.doi.org/10.1016/582 j.pss.2006.04.23.

Bougher, S.W., Brecht, A., Schulte, R., Fischer, J., Parkinson, C.D., Mahieux, A., Wilquet, V., Vandaele, A.C., 2015. Upper atmosphere temperature structure at the Venusian terminators: a comparison of SOIR and VTGCM results. Planet. Space Sci., http://dx.doi.org/10.1016/j.pss.2015.01.012

Brecht, A., Bougher, S.W., Gerard, J.-C., Parkinson, C., Rafkin, S., Foster, B., 2011. Understanding the variability of nightside temperatures, NO UV and O_2 IR nightglow emissions in the Venus upper atmosphere. J. Geophys. Res. 116, E08004. http://dx.doi.org/10.1029/2010JE003770.

Clancy, R.T., Muhleman, D.O., 1991. Long-term (1979–1990) changes in the thermal, dynamical, and compositional structure of the Venus mesosphere as inferred from microwave spectral line observations of ^{12}CO, ^{13}CO, and $C^{18}O$. Icarus 89, 129–146.

de Kok, R., Irwin, P.G.J., Tsang, C.C.C., Piccioni, G., Drossart, P., 2011. Scattering particles in nightside limb observations of Venus' upper atmosphere by Venus Express VIRTIS. Icarus 211, 51–57.

English, J.M., Toon, O.B., Mills, M.J., Yu, F., 2011. Microphysical simulations of new particle formation in the upper troposphere and lower stratosphere. Atmos. Chem. Phys. 11, 9303–9322.

Esposito, L.W., Knollenberg, R.G., Marov, M.Y., Toon, O.B., Turco, R.P., 1983. The clouds and hazes of Venus In: Hunten, D.M., et al. (Eds.), Venus. Univ. of Ariz. Press, Tucson, USA, pp. 484–564.

Gao, P., Zhang, X., Crisp, D., Bardeen, C.G., Yung, Y.L., 2014. Bimodal distribution of sulphuric acid aerosols in the upper haze of Venus. Icarus 231, 83–98.

Häusler, B., Pätzold, M., Tyler, G.L., Simpson, R.A., Bird, M.K., Dehant, V., Barriot, J.-P., Eidel, W., Mattei, R., Remus, S., Selle, J., Tellmann, S., Imamura, T., 2006. Radio science investigations by VeRa onboard the Venus Express spacecraft. Planet. Space Sci. 54, 1315–1335.

Häusler, B., Pätzold, M., Tyler, G.L., Barriot, J.-P., Bird, M.K., Dehant, V., Hinson, D.P., Simpson, R.A., Treumann, R.A., Eidel, W., Mattei, R., Rosenblatt, P., Remus, S., Selle, J., Tellmann, S., 2007. Venus Atmospheric, Ionospheric, Surface and Interplanetary Radio-Wave Propagation Studies with the VeRa Radio-Science Experiment. ESA Publication, SP-1295, p. 30.

Hunten, D.M., Turco, R.P., Toon, O.B., 1980. Smoke and dust particles of meteoric origin in the mesosphere and stratosphere. J. Atmos. Sci. 37, 1342–1357.

Ignatiev, N.I., Moroz, V.I., Moshkin, B.E., Ekonomov, V.I., Gnedykh, A.V., Grigoriev, A. V., Khatuntsev, I.V., 1997. Water vapour in the lower atmosphere of Venus: a new analysis of optical spectra measured by entry probes. Planet. Space Sci. 45, 427–438.

Imamura, T., Hashimoto, G.L., 2001. Microphysics of Venusian clouds in rising tropical air. J. Atmos. Sci. 58, 3597–3612.

Jacobson, M.Z., Turco, R.P., 1994. Modeling coagulation among particles of different composition and size. Atmos. Environ. 28, 1327–1338.

James, E.P., Toon, O.B., Schubert, G., 1997. A numerical microphysical model of the condensational Venus cloud. Icarus 129, 147–171.

Kalashnikova, O., Horanyi, M., Thomas, G.E., Toon, O.B., 2000. Meteoric smoke production in the atmosphere. Geophys. Res. Lett. 27, 3293–3296.

Kawabata, K., Coffeen, D.L., Hansen, J.E., Lane, W.A., Sato, M., Travis, L.D., 1980. Cloud and haze properties from Pioneer Venus polarimetry. J. Geophys. Res. 85, 8129–8140.

Knollenberg, R.G., Hunten, D.M., 1980. The microphysics of the clouds of Venus: results of the Pioneer Venus particle size spectrometer experiment. J. Geophys. Res. 85, 8039–8058.

Kolodner, M.A., Steffes, P.G., 1998. The microwave absorption and abundance of sulphuric acid vapour in the Venus atmosphere based on new laboratory measurements. Icarus 132, 151–169.

Krasnopolsky, V.A., 1983. Venus spectroscopy in the 3000-8000 A region by Veneras 9 and 10 In: Hunten, D.M., et al. (Eds.), Venus. Univ. of Ariz. Press, Tucson, USA, pp. 459–483.

Krasnopolsky, V.A., Parshev, V.A., 1983. Photochemistry of the Venus atmosphere In: Hunten, D.M., et al. (Eds.), Venus. Univ. of Ariz. Press, Tucson, USA, pp. 431–458.

Krasnopolsky, V.A., Pollack, J.B., 1994. H_2O–H_2SO_4 system in Venus' clouds and OCS, CO, and H_2SO_4 profiles in Venus' troposphere. Icarus 109, 58–78.

Krasnopolsky, V.A., 2011. Vertical profile of H_2SO_4 vapor at 70–110 km on Venus and some related problems. Icarus 215, 197–203.

Krasnopolsky, V.A., 2012. A photochemical model for the Venus atmosphere at 47-112 km. Icarus 218, 230–246. http://dx.doi.org/10.1016/j.icarus.2011.11.012.

Linkin, V.M., Kerzhanovich, V.V., Lipatov, A.N., Pichkadze, K.M., Shurupov, A.A., Terterashvili, A.V., Ingersoll, A.P., Crisp, D., Grossman, A.W., Young, R.E., Seiff, A., Ragent, B., Blamont, J.E., Elson, L.S., Preston, R.A., 1986. Vega balloon dynamics and vertical winds in the Venus middle cloud region. Science 231, 1417–1419.

Lyons, J.R., 2008. An estimate of the equilibrium speciation of sulphur vapour over solid sulphur and implications for planetary atmospheres. J. Sulphur Chem. 29, 269–279.

Markiewicz, W.J., Titov, D.V., Limaye, S.S., Keller, H.U., Ignatiev, N., Jaumann, R., Thomas, N., Michalik, H., Moissl, R., Russo, P., 2007. Morphology and dynamics of the upper cloud layer of Venus. Nature 450, 633–636.

McGouldrick, K., Toon, O.B., 2007. An investigation of possible causes of the holes in the condensational Venus cloud using a microphysical cloud model with a radiative-dynamical feedback. Icarus 191, 1–24.

McGouldrick, K., Toon, O.B., Grinspoon, D.H., 2011. Sulphuric acid aerosols in the atmosphere of the terrestrial planets. Planet. Space Sci. 59, 934–941.

Mahieux, A., Vandaele, A.C., Drummond, R., Robert, S., Wilquet, V., Fedorova, A., Bertaux, J.L., 2010. Densities and temperatures in the Venus mesosphere and lower thermosphere retrieved from SOIR onboard Venus Express: retrieval technique. J. Geophys. Res. 115, E12014.

Mahieux, A., Vandaele, A.C., Robert, S., Wilquet, V., Drummond, R., Montmessin, F., Bertaux, J.L., 2012. Densities and temperatures in the Venus mesosphere and lower thermosphere retrieved from SOIR on board Venus Express: carbon dioxide measurements at the Venus terminator. J. Geophys. Res. (Planets) 117, E07001. http://dx.doi.org/10.1029/2012JE004058.

Mahieux, A., Vandaele, A.-C., Bougher, S.W., Yelle, R.V., Drummond, R., Robert, S., Wilquet, V., Piccialli, A., Montmessin, F., Tellmann, S., Patzold, M., Hausler, B., Bertaux, J.-L., 2015. Update of the Venus density and temperature profiles at high altitude measured by SOIR on board Venus Express. Planet. Space Sci., http://dx.doi.org/10.1016/j.pss.2015.02.002

Mills, F.P., Allen, M., 2007. A review of selected issues concerning the chemistry in Venus' middle atmosphere. Plan. Space Sci., http://dx.doi.org/10.1016/j.pss.2007.01.012

Mills, F.P., Esposito, L.W., Yung, Y.L., 2007. Atmospheric composition, chemistry, and clouds In: Esposito, L.W., et al. (Eds.), Exploring Venus as a Terrestrial Planet. American Geophysical Union, Washington DC, USA, pp. 73–100.

Oschlisniok, J., Häusler, B., Pätzold, M., Tyler, G.L., Bird, M.K., Tellmann, S., Remus, S., Andert, T., 2012. Microwave absorptivity by sulphuric acid in the Venus atmosphere: first results from the Venus Express Radio Science experiment VeRa. Icarus 22, 940–948.

Parkinson, C.D., Yung, Y.L., Esposito, L., Gao, P., Bougher, S.W., Hirtzig, M., 2015. Photochemical Control of the Distribution of Venusian Water. Planet. Space Sci, http://dx.doi.org/10.1016/j.pss.2015.02.015.

Pätzold, M., Häusler, B., Bird, M.K., Tellmann, S., Mattei, R., Asmar, S.W., Dehant, V., Eidel, V., Imamura, W., Simpson, T, R.A., Tyler, G.L., 2007. The structure of Venus' middle atmosphere and ionosphere. Nature 450, 657–660.

Peter, K., Pätzold, M., Molina-Cuberos, G., Witasse, O., Gonzalez-Galindo, F., Withers, P., Bird, M.K., Häusler, B., Hinson, D.P., Tellmann, S., Tyler, G.L., 2014. The dayside ionospheres of Mars and Venus: comparing a one-dimensional photochemical model with MaRS (Mars Expresss) and VeRa (Venus Express) observations. Icarus 233, 66–82.

Seiff, A., Schofield, J.T., Kliore, A.J., Taylor, F.W., Limaye, S.S., Revercomb, H.E., Sromovsky, L.A., Kerzhanovich, V.V., Moroz, V.I., Ya., Marov M., 1985. Models of the structure of the atmosphere of Venus from the surface to 100 kilometers altitude. Adv. Space Res. 5, 3–58.

Tellmann, S., Pätzold, M., Häusler, B., Bird, M.K., Tyler, G.L., 2009. Structure of the Venus neutral atmosphere as observed by the Radio Science experiment VeRa on Venus Express. J. Geophys. Res. 114 (E00B36), 19.

Tellmann, S., Häusler, B., Hinson, D.P., Tyler, G.L., Andert, T.P., Bird, M.K., Imamura, T., Pätzold, M., Remus, Sand, 2012. Small-scale temperature fluctuations seen by the VeRa Radio Science Experiment on Venus Express. Icarus 221, 471–480.

Toon, O.B., Turco, R.P., Pollack, J.B., 1982. The ultraviolet absorber on Venus: amorphous sulphur. Icarus 51, 358–373.

Toon, O.B., Turco, R.P., Westphal, D., Malone, R., Liu, M.S., 1988. A multidimensional model for aerosols: description of computational analogs. J. Atmos. Sci. 45, 2123–2143.

Toon, O.B., Turco, R.P., Jordan, J., Goodman, J., Ferry, G., 1989. Physical processes in polar stratospheric ice clouds. J. Geophys. Res. 94, 11359–11380.

Turco, R.P., Hamill, P., Toon, O.B., Whitten, R.C., Kiang, C.S., 1979. A one-dimensional model describing aerosol formation and evolution in the stratosphere: I. Physical processes and mathematical analogs. J. Atmos. Sci. 36, 699–717.

Wilquet, V., Drummond, R., Mahieux, A., Robert, S., Vandaele, A.C., Bertaux, J.-L., 2012. Optical extinction due to aerosols in the upper haze of Venus: four years of SOIR/VEX observations from 2006 to 2010. Icarus 217, 875–881.

Wilquet, V., Fedorova, A., Montmessin, F., Drummond, R., Mahieux, A., Vandaele, A. C., Villard, E., Korablev, O., Bertaux, J.-L., 2009. Preliminary characterization of the upper haze by SPICAV/SOIR solar occultation in UV to mid-IR onboard Venus Express. J. Geophys. Res. 114 (E00B42), 13.

Wilson, C.F., Guerlet, S., Irwin, P.G.J., Tsang, C.C.C., Taylor, F.W., Carlson, R.W., Drossart, P., Piccioni, G., 2008. Evidence for anomalous cloud particles at the poles of Venus. J. Geophys. Res.-Planets, 113.

Yamamoto, M., Tanaka, H., 1998. The Venusian Y-shaped cloud pattern based on an aerosol-transport model. J. Atmos. Sci. 55, 1400–1426.

Yamamoto, M., Takahashi, M., 2006. An aerosol transport model based on a two-moment microphysical parametrization in the Venus middle atmosphere: model description and preliminary experiments. J. Geophys. Res. 111 (E08002), 12.

Yung, Y.L., DeMore, W.B., 1982. Photochemistry of the stratosphere of Venus: implications for atmospheric evolution. Icarus 51, 199–247.